



**HAL**  
open science

# Plasticity of the xylem vulnerability to embolism in *Populus tremula* x *alba* relies on pit quantity properties rather than on pit structure

Cedric Lemaire, Nicole Brunel-Michac, Jérémie Santini, Liliane Berti, Julien Cartailleur, Pierre Conchon, Eric Badel, Stéphane Herbette

## ► To cite this version:

Cedric Lemaire, Nicole Brunel-Michac, Jérémie Santini, Liliane Berti, Julien Cartailleur, et al.. Plasticity of the xylem vulnerability to embolism in *Populus tremula* x *alba* relies on pit quantity properties rather than on pit structure. *Tree Physiology*, 2021, 41 (8), pp.1384-1399. 10.1093/treephys/tpab018 . hal-03141908

**HAL Id: hal-03141908**

**<https://hal.inrae.fr/hal-03141908>**

Submitted on 15 Feb 2021

**HAL** is a multi-disciplinary open access archive for the deposit and dissemination of scientific research documents, whether they are published or not. The documents may come from teaching and research institutions in France or abroad, or from public or private research centers.

L'archive ouverte pluridisciplinaire **HAL**, est destinée au dépôt et à la diffusion de documents scientifiques de niveau recherche, publiés ou non, émanant des établissements d'enseignement et de recherche français ou étrangers, des laboratoires publics ou privés.

1 **Research Paper**

2 **Plasticity of the xylem vulnerability to embolism in *Populus tremula* x *alba* relies on pit**  
3 **quantity properties rather than on pit structure.**

4 Cédric Lemaire <sup>1</sup>, Yann Quilichini <sup>2</sup>, Nicole Brunel-Michac <sup>1</sup>, Jérémie Santini <sup>2</sup>, Liliane Berti <sup>2</sup>,  
5 Julien Cartailier <sup>1</sup>, Pierre Conchon <sup>1</sup>, Éric Badel <sup>1</sup> and Stéphane Herbette <sup>1</sup>.

6 <sup>1</sup> Université Clermont Auvergne, INRAE, PIAF, F-63000 Clermont-Ferrand, France.

7 <sup>2</sup> UMR 6134 SPE, CNRS-Università di Corsica, 20250 Corti, France

8

9 **Keywords**

10 Acclimation, anatomy, cavitation, hydraulic, phenotypic plasticity, Poplar, shade, water stress,  
11 X-ray microCT.

12

13 **Running head**

14 Structural determinants of plasticity of embolism resistance

15

16 **Full address of the corresponding author**

17 Stéphane Herbette

18 UMR INRAE/UCA 547 PIAF

19 Université Clermont Auvergne, Campus Universitaire des Cézeaux,

20 1 Impasse Amélie Murat,

21 TSA 60026, 63178 AUBIERE Cedex

22 FRANCE

23 Stephane.Herbette@uca.fr

**24 Abstract**

25 Knowledge on variations of drought resistance traits are needed to predict the potential of trees  
26 to acclimate to coming severe drought events. Xylem vulnerability to embolism is a key  
27 parameter related to such droughts, and its phenotypic variability relies mainly on  
28 environmental plasticity. We investigated the structural determinants controlling the plasticity  
29 of vulnerability to embolism, focusing on the key elements involved in the air bubble entry in  
30 vessels, especially the inter-vessel pits. Poplar saplings (*Populus tremula x alba*) grown in  
31 contrasted water availability or light exposure exhibited differences in vulnerability to  
32 embolism ( $P_{50}$ ) in a range of 0.76 MPa. We then characterized the structural changes in features  
33 related to pit quantity and pit structure, from the pit ultrastructure to the organization of xylem  
34 vessels, using different microscopy techniques (TEM, SEM, LM). A multispectral combination  
35 of X-ray microtomography and light microscopy analysis allowed measuring the vulnerability  
36 of each single vessel and testing some of the relationships between structural traits and  
37 vulnerability to embolism inside the xylem. The pit ultrastructure did not change, whereas the  
38 vessel dimensions increased with vulnerability to embolism and the grouping index and fraction  
39 of inter-vessel cell wall both decreased with vulnerability to embolism. These findings hold  
40 when comparing between trees, or between the vessels inside the xylem of an individual tree.  
41 These results evidenced that plasticity of vulnerability to embolism in hybrid poplar occurs  
42 through changes in the pit quantity properties such as pit area and vessel grouping rather than  
43 on the pit structure.

**44 Keywords**

45 Acclimation, anatomy, cavitation, hydraulic, phenotypic plasticity, Poplar, shade, water stress,  
46 X-ray microCT.

47

## 48 **Introduction**

49 According to the cohesion-tension theory (Steudle 2001), the water columns in the xylem are  
50 under tension, a metastable state. When this tension increases during droughts, the water  
51 columns are more prone to break, because of cavitation: vapour bubbles invade the impacted  
52 vessels and spread, impeding function and leading to a loss of xylem conductance. When the  
53 loss of conductance reaches a threshold (around 90%), the distal organs are not supplied with  
54 water anymore leading to death (Barigah et al. 2013). For woody species, drought-induced  
55 death is more likely due to xylem hydraulic failure (Anderegg et al. 2015, 2016, Adams et al.  
56 2017) caused by embolism in the xylem conduits, even if other processes can also contribute to  
57 this death (Hammond et al. 2019) such as the carbon starvation (Hartmann et al. 2015).

58 A global analysis pointed out the narrow hydraulic safety margin at which woody species  
59 usually operate (Choat et al. 2012); inferring that research is needed on the variability of  
60 vulnerability to embolism. Within-species variability for vulnerability to embolism was shown  
61 for many tree species (e.g. Martínez-Vilalta et al. 2009, Herbette et al. 2010). The genetic  
62 variability for this trait is rather limited in both natural populations (Lamy et al. 2011,  
63 Wortemann et al. 2011) and cultivated species (Jinagool et al. 2015, 2018). This trait would be  
64 genetically canalized (Lamy et al. 2012) and varies mainly via plasticity due to environmental  
65 factors (Herbette et al. 2010). Plasticity of vulnerability to embolism was reported mainly under  
66 water stress, with wood formed under drier conditions being less vulnerable (Awad et al. 2010,  
67 Fichot et al. 2010, Plavcová and Hacke 2012). Other conditions such as shade or fertilization  
68 were associated to an increase in vulnerability to embolism (Cooke et al. 2005, Barigah et al.  
69 2006, Plavcová and Hacke 2012). However, information is scarce on the determinants of  
70 plasticity of vulnerability to embolism. The structural determinants need to be deciphered first,  
71 before searching for their genetic control, as it can be complex to decipher the role of candidate  
72 genes (Allario et al. 2018).

73 In angiosperms, water flows between xylem vessels through bordered pits. These pits are  
74 openings in the secondary cell wall that allow water to flow between vessels while they prevent  
75 air seeding from neighbouring air-filled vessels. Pits have been identified as the key structures  
76 for vulnerability to embolism (Lens et al. 2013; Jansen et al. 2018, Kaack et al. 2019). Thus,  
77 we assume that the acclimation of vulnerability to embolism to environmental conditions would  
78 involve changes in the pit quantity and/or structure, i.e. at pit and/or vessel scales (Lens et al.  
79 2013). The key role of the pit ultrastructure in vulnerability to embolism has been evidenced in  
80 several studies (e.g. Choat et al. 2008, Lens et al. 2011, Tixier et al. 2014), especially the pit  
81 membrane (Jansen et al. 2009, Li et al. 2016, Kaack et al. 2019). There is a well-established  
82 correlation between pit membrane thickness and vessel resistance to embolism in angiosperms  
83 (Lens et al. 2011, Plavcová and Hacke 2012, Scholz et al. 2013a, Schuldt et al. 2016). A  
84 mechanistic explanation has been provided through the recent discoveries on the three-  
85 dimensional structure of the pit membrane (Kaack et al. 2019, 2020). Pit membrane is a porous  
86 medium with series of various pore constrictions influencing the air seeding, and constriction  
87 sizes decreased with increasing pit membrane thickness. Vulnerability to embolism is also  
88 dependent on pit quantity parameters such as the pit area or the vessel connectivity and thus on  
89 vessel dimensions and three dimensional organization (Lens et al. 2013). Zimmermann and Jeje  
90 (1981) already pointed out that the hydraulic vulnerability could be related to the vessel volume  
91 that varies depending on both their diameter (Tyree et al. 1994) and their length (Scholz et al.  
92 2013a). Several studies demonstrated a relationship between vulnerability to embolism and  
93 vessel diameter (Wheeler et al. 2005, Hacke et al. 2006, Maherali et al., 2006; Awad et al. 2010,  
94 Hajek et al., 2014). However, other studies failed to detect such a relationship (Lens et al., 2011,  
95 Scholtz et al. 2013 a, Schuldt et al. 2016). Such discrepancy between findings can be explained  
96 by uncertainties about the relationship between vessel diameter and pit area. More, one has to  
97 acknowledge that vulnerability to embolism is not controlled exclusively by either pit quantity

98 parameters or pit structure (Choat and Pittermann 2009). The three-dimensional organization  
99 of the xylem network would also influence the vulnerability to embolism, as shown in  
100 theoretical and empirical analyses (Loepfe et al. 2007, Mrad et al. 2018). The relationship  
101 between vulnerability to embolism and pit properties has been intensively studied at the inter-  
102 specific level, whereas the determinants of plasticity of vulnerability to embolism remain poorly  
103 investigated at the intraspecific level (Schuldt et al. 2016). For example, in poplar, Plavcová et  
104 al. (2011) showed that shading caused an increase in vulnerability to embolism associated with  
105 a decrease in both pit membrane thickness and vessel diameter, whereas Awad et al. 2010  
106 showed that a reduced watering induced a decrease in vulnerability to embolism linked with a  
107 decrease in vessel diameter.

108 In this work, we investigated the relationship between the plasticity of vulnerability to  
109 embolism and changes in structures related to pit properties at different anatomical levels on  
110 young poplars (*Populus tremula x alba*). We grew saplings of a poplar clone under three  
111 contrasted environmental conditions for two factors (water and light availability) known to  
112 induce variation of vulnerability to embolism. Then, their xylem anatomy was analysed in  
113 relation to the changes in vulnerability to embolism using different approaches. Transmission  
114 Electron Microscopy (TEM) allowed investigations on the pit ultrastructure. Parameters related  
115 to the pit-field were measured using Scanning Electron Microscopy (SEM). We also measured  
116 pit quantity parameters related to vessel dimensions and vessel connectivity using light  
117 microscopy and silicon injections. Then, an approach using direct observation of embolism  
118 spreading inside the xylem by X-ray microtomography allowed to analyse the relationships  
119 between structural traits and vulnerability to embolism at the vessel level.

120

## 121 **Materials and Methods**

### 122 **Plant material and growth conditions**

123 *Plant Material.* Saplings of hybrid poplar (*Populus tremula x alba* clone INRA 717-1B4) were  
124 propagated clonally *in vitro* on Murashige and Skoog medium on December 2016. Plantlets  
125 were transferred in hydroponic solution on February 2017 and grown in a controlled  
126 environment room: 16 h daylight at 21-22 °C, 40  $\mu\text{mol}\cdot\text{m}^{-2}\cdot\text{s}^{-1}$  and 18-19 °C night, at  $70 \pm 10$  %  
127 relative humidity. On March 2017, plants were transferred in 1 Litre pots filled with potting  
128 soil (Humustar Terreaux, Champeix, France) with a composition of 25 % brown peat, 40 %  
129 blond peat and 35 % pine bark dust. The pots were placed in a greenhouse at the INRAE  
130 research station of Clermont-Ferrand, France (site of Crouël; N 45°77', E 3°14'; 300 m *a.s.l.*).  
131 After 20 days, plants were transferred in 10 L pots filled with potting soil. They were regularly  
132 watered at soil field capacity. Each pot weighted  $6.4 \pm 0.4$  kg. Ten days later, the specific  
133 experimental growth conditions were applied (see next). After one month of growth, stems were  
134 cut at 50 cm height. The growth of a new apical bud occurred in May 2017, and any additional  
135 bud was removed. Thus, a single stem completely grew under the new environmental  
136 conditions.

137 *Experimental setup.* Plants were split in three groups submitted to different growth conditions:  
138 (i) “control” plants grew under full sunlight and watered at soil field capacity; (ii) ”droughted”  
139 plants grew under full sunlight and watered at 25-30 % of soil field capacity; (iii) ”shaded”  
140 plants shaded by a shadehouse that intercepted 30 % of incident light and watered at soil field  
141 capacity. For the nine droughted plants, an irrigation at 25-30 % of soil field capacity was kept  
142 constant in each pot individually using balances and automatic valves for irrigation as described  
143 in Niez et al. (2019). We measured the light interception by the shadehouse by comparing for  
144 two months the light intensities recorded with two sensors (PAR/CBE 80, Solems, Palaiseau,  
145 France) placed inside the shadehouse and two sensors placed outside. The level of water stress  
146 was set to be the most restrictive while allowing growth to produce acclimatized xylem and  
147 enough plant material for further analyses. The stem diameter was continuously measured using

148 a LVDT sensor (Linear Variable Differential Transformer) on three droughted, two control and  
149 three shaded plants. Plant height was measured using a measuring tape.

150 One month before and the day before the tree sampling, predawn water potential ( $\Psi_{pd}$ ) was  
151 measured on every plant 1 hour before the sunrise using a pressure chamber (1505D, PMS  
152 Instrument, Albany, OR, USA, Scholender et al. 1965). The same day, midday water potential  
153 ( $\Psi_{mid}$ ) was measured at the solar noon, between 12:00 and 2:00 PM.

154 *Sampling protocol.* The sampling was performed on 28 August 2017. Plants were cut at 20 cm  
155 height. The plant shoot was immersed underwater and the 30 cm of the top were removed as it  
156 lacks significant secondary xylem. Then, the following stem segments were sampled, from  
157 basal to apical direction:

158 i) the 30 cm long basal part of the stem was removed because it was not fully grown under  
159 acclimation conditions;

160 ii) the first 50 cm long of the newly developed stem under the acclimation conditions was  
161 wrapped in wet paper, put in a plastic bag and stored at 4 °C until measurements of vulnerability  
162 to embolism and vessel length;

163 iii) the above segment of 6 cm long was devoted to microscopy analyses. It was split into three  
164 subsamples using a razor blade: two segments of 1 cm long were prepared for light microscopy  
165 and TEM observations. A third segment of 4 cm long was prepared for SEM observations;

166 iv) if the stem was long enough, an additional segment of 50 cm long was wrapped in wet paper  
167 in a plastic bag, and stored at 4 °C for measurements of specific conductivity ( $K_S$ ) and for  
168 additional measurements of vulnerability to embolism;

169 v) the last 10 cm long was kept wrapped in humid paper for a native embolism measurement  
170 performed on the sampling day.

171 Leaves were sampled under water and the total leaf area (LA) per plant was measured in the  
172 day using an area-meter (Li-3100c, Li-Cor Biosciences, Lincoln, NE, USA).



173 After the sampling, plants were kept in the greenhouse, during the winter 2017. On March 2018,  
 174 they started growing, still under the same environmental conditions as described above, and on  
 175 July 2018 we performed a second sample collection: plants were cut at 25 cm height. Then the  
 176 30 cm long basal part of the stem was cut underwater. A 50 cm long sample was wrapped in  
 177 wet paper and stored in a plastic bag at 4 °C for measurements of specific conductivity ( $K_S$ ).

#### 178 **Hydraulic traits measurements:**

179 *Vulnerability to embolism.* The 50 cm long stem segment was shortened underwater at 43 cm  
 180 long using a razor blade. Then, the vulnerability to embolism was assessed using the Cavitron  
 181 technique (Cochard 2002, Cochard et al. 2005). A centrifugal force increases water tension in  
 182 branch segment while a specific optical device allows the continuous measurement of the loss  
 183 of conductance (Cochard et al. 2009). A vulnerability curve was built by plotting the percentage  
 184 loss xylem conductance (PLC) vs. xylem water pressure ( $P$ ). A sigmoidal function was used to  
 185 fit each curve using the equation 1 (Pammenter and Willigen 1998).

$$186 \quad \text{PLC} = \frac{100}{1 + e^{\frac{S(P - P_{50})}{25}}} \quad (1)$$

187 Where  $P_{50}$  is the pressure causing 50 % loss of conductance, and  $S$  is the slope of the curve at  
 188 this point.

189 *Specific conductivity.* Stem segments of 50 cm long were shortened underwater at a length  
 190 ( $L_{\text{stem}}$ ) of 40 cm long using a razor blade for droughted ( $n = 8$ ), control ( $n = 9$ ) and shaded ( $n =$   
 191 9) plants. The apical end of the sample was sealed to a tubing system (polytetrafluoroethylene  
 192 film) and plugged to an embolism meter (Xyl'em, Bronkhorst, Montigny les Cormeilles,  
 193 France). The initial conductance ( $K_i$ ) was then measured under low pressure (2 to 7 kPa) using  
 194 a solution of 10 mM KCl and 1 mM CaCl<sub>2</sub>. The xylem area  $A_X$  of the distal end of the sample  
 195 was measured on a cross section using a scanner (V800, Epson, Nagano, Japan). The  
 196 measurement of  $A_X$  was performed on the scanned image using the ImageJ software (version

197 v.1.52c) (Schneider et al. 2012). The Specific Conductivity  $K_S$  was defined according to  
 198 equation 2.

$$199 \quad K_S = \frac{K_i \times L_{stem}}{A_x} \quad (2)$$

200 *Native Embolism*. The native embolism of the stem segments of 10 cm long were measured on  
 201 the sampling day for droughted (n = 9), control (n = 5) and shaded (n = 6) plants. Each sample  
 202 was shortened underwater using a razor blade to a length of 8 cm. Then, the initial conductance  
 203 ( $K_i$ ) was measured under low pressure (2 to 7 kPa) with the same method and the same solution  
 204 as for specific conductivity. Then, the sample was flushed with the same solution twice for  
 205 5 min under high pressure (0.1 to 0.2 MPa) in order to remove the air embolism. A new  
 206 measurement of conductance without embolism indicated the maximum conductance ( $K_{max}$ ) of  
 207 the sample. The native embolism was calculated according to the equation 3.

$$208 \quad \text{Native Embolism} = \left(1 - \frac{K_i}{K_{max}}\right) \times 100 \quad (3)$$

### 209 **Light microscopy**

210 Samples of 1 cm long were cut into 3 x 3 mm<sup>2</sup> blocks then they were immersed in Karnovsky's  
 211 fixative solution under vacuum for 30 min, then stored at 4 °C in the fixative solution up to the  
 212 next step. Then, they were dehydrated in an ethanol series (50, 70, 80, and 95 %) and embedded  
 213 in LR White resin. Transverse slices of 2 to 3 µm thick were cut using an ultramicrotome (Om  
 214 U2, Reichert, Vienna, Austria). Sections were stained with 1 % (w/v) toluidine blue, washed 4  
 215 times with water and mounted in Eukitt (Sigma-Alrich, St-Louis, MO, USA). Images were  
 216 processed using a microscope (Zeiss Axio Observer Z1), a digital camera (AxioCam MRc) and  
 217 Zen imaging software system (Zeiss, Jena, Germany).

218 Image analyses were performed using ImageJ software with a home-made semi-automated  
 219 procedure. The vessel diameter ( $D_v$ ) was estimated to be the diameter of the circle having the  
 220 same area as the vessel lumen (for the symbols, see Table 1). The total vessel wall perimeter in  
 221 contact with other vessel was measured using the Feret diameters. The vessel diameters were

222 increased by five pixels using dilate function and if dilated vessels overlapped, they were  
223 considered to be in contact. The maximum Feret diameter of the overlapping area was  
224 considered to be their length of wall in contact. From there, the contact fraction ( $F_c$ ) was  
225 measured for each vessel as the ratio of length of wall in contact with other vessels over the  
226 perimeter of the vessel. Vessels that shared wall were assigned to the same group. As a result,  
227 the two-dimensional grouping index (GI) was the mean number of vessels per group and the  
228 solitary index (SI) as the ratio of the number of solitary vessels to the total number of vessels.  
229 These parameters were measured for each individual slice containing a mean of 850 vessels,  
230 for droughted ( $n = 9$ ), control ( $n = 5$ ) and shaded ( $n = 6$ ) plants.

### 231 **Vessel length**

232 The vessel length was measured by the silicon injection method (Sperry et al. 2005, Scholz et  
233 al. 2013b) on the samples already used for Cavitron technique, after five months of drying at  
234 room temperature. A fluorescent optical brightener (CAS number: 7128-64-5, Sigma-Aldrich,  
235 St-Louis, MO, USA) was mixed in chloroform (1 % w/w) and added to a volume of silicon  
236 (BLUESIL RTV-141 A, Bluestar Silicones, Lyon, France) with a proportion of one drop of  
237 solution per gram of silicon. A Silicone hardener (BLUESIL RTV-141 B, Bluestar Silicones)  
238 was added to the mixture in 1:10 proportion. The mixture was then injected under pressure (300  
239 to 400 kPa) basipetally in the stem sample using a pressure chamber during at least 8 hours.  
240 After silicone hardening (3 days at room temperature), the samples were cut 5 mm far from the  
241 injection point; then every 20 mm. For each segment, a 25  $\mu\text{m}$  thick slice was cut using a rotary  
242 microtome (RM2165, Leica Microsystems, Wetzlar, Germany). Cross sections were dyed with  
243 Astra Blue and mounted with a glycerol medium.

244 Images were obtained using a fluorescence microscope (Axio Observer Z1) equipped with a  
245 300 to 400 nm band pass excitation filter, a digital camera (AxioCam 506), Zen imaging  
246 software system (Zeiss, Jena, Germany) and analysed using the ImageJ software. Fluorescent

247 vessels highlighted the open vessels, while white light allowed counting the total number of  
 248 vessels. The decrease of the ratio of open vessels ( $N_x$ ) (*i.e.* fluorescent vessels) to the total  
 249 number of vessels ( $N_0$ ) over the distance ( $x$ ) from the end of the sample followed an exponential  
 250 decay function (equation 4) where  $k$  is the best-fit extinction coefficient (Cohen et al. 2003).

$$251 \quad N_x = N_0 \times e^{-kx} \quad (4)$$

252 The fraction of conduits of length  $x$  ( $P(x)$ ) is obtained by multiplying  $x/N_0$  to the second  
 253 derivative of equation 4 (Wheeler et al. 2005):

$$254 \quad P(x) = x \times k^2 \times e^{-kx} \quad (5)$$

255 The continuous cumulative function of vessel length ( $L_v$ ) probability is a function given in the  
 256 equation 6.

$$257 \quad f(x) = \int_0^{L_v} x k^2 \cdot e^{-kx} dx \quad (6)$$

258 When this cumulative function is equal to 0.5, this gives the median value of vessel length  
 259 ( $L_v$ ) (equation 7).

$$260 \quad f(L_v) = - (kL_v + 1) \cdot e^{-kL_v} + 1 = 0.5 \quad (7)$$

261 The solution of the equation 7 gives the median vessel length  $L_v = 1.678/k$ . This vessel  
 262 length was estimated for 7 droughted, 5 control and 5 shaded stem samples.

### 263 **Transmission Electron Microscopy**

264 Fresh samples of 1 cm long were cut into 2 to 4 mm<sup>3</sup> blocks, immersed in Karnovsky's fixative  
 265 solution under vacuum for 30 min, then stored at 4 °C in the fixative solution for 3 weeks.  
 266 Blocks were recut into 1 to 2 mm<sup>3</sup> pieces, then they were fixed secondarily for 4 hours at  
 267 ambient temperature in a 0.1M phosphate-buffered osmium tetroxide solution (1 %), pH 7.4.  
 268 Then, they were dehydrated in an ethanol series (25, 50, 70, 100, and 100 %) and embedded in  
 269 Epoxy resin using Epoxy medium kit (Sigma-Aldrich, St-Louis, MO, USA). Then, ultra-thin  
 270 sections (60-90 nm) were cut using an ultramicrotome (PowerTome PC, RMC Boeckeler,  
 271 Tucson, AZ, USA). The sections were placed on 200- and 300-mesh copper grids and stained

272 with contrast solutions: UranylLess (Delta Microscopies, Mauressac, France) and lead citrate.  
 273 Sections were observed using a transmission electron microscope (H-7650, Hitachi High-  
 274 Technologies Corporation, Tokyo, Japan) at a voltage of 80 kV. Measurements of pit features  
 275 were performed on images with pits showing two apertures. Pits were characterized for their  
 276 diameter ( $D_p$ ), their aperture diameter ( $D_a$ ), their chamber depth ( $L_p$ ) and their membrane  
 277 thickness ( $T_m$ ). For each pit,  $D_a$  was the mean of two measurements while  $L_p$  and  $T_m$  were the  
 278 mean of four measurements. Pit features were measured for five individual trees for each  
 279 growth condition, with at least 10 pits measured per individual tree.

### 280 **Scanning Electron Microscopy**

281 Fresh samples were fixed in 3 % glutaraldehyde and stored at 4 °C for at least 1 month. Samples  
 282 of 4 cm long were cut longitudinally and then dehydrated in an ethanol series (30, 50, 75, and  
 283 100 %). After dehydration, samples were immersed in a 1:1 solution hexamethyldisilazane  
 284 (HMDS) + ethanol 100 % for 30 min and immersed in pure HDMS for 30 min. After air drying  
 285 overnight under a hood, the samples were mounted on aluminium stubs with carbon double-  
 286 sided adhesive disks, coated with gold/palladium in a sputter coater (SC7640, Quorum  
 287 Technologies Ltd, Newhaven, U.K.), and finally observed using a scanning electron  
 288 microscope (S-3400N, Hitachi High-Technologies Corporation, Tokyo, Japan) at a voltage of  
 289 5 kV. The portion of area covered by bordered pits in each inter-vessel pit-field ( $F_{pf}$ ) was then  
 290 measured by image analysis using the ImageJ software. Five samples were measured per growth  
 291 condition, and seven pit-fields were characterized per sample.

### 292 **Estimation of supplementary hydraulic and structural traits**

293 Theoretical conductivities ( $K_{s\_theo}$ ) of all samples characterized by light microscopy were  
 294 calculated according to Scholz et al. (2013b) and converted into  $\text{g}\cdot\text{s}^{-1}\cdot\text{MPa}^{-1}\cdot\text{m}^{-1}$  (equation 8).

$$295 \quad K_{s\_theo} = \frac{\sum \frac{\pi D_v^4}{128 \eta}}{A_x} \times \rho \quad (8)$$

296 Where  $\eta$  is the viscosity index of water ( $1.002 \times 10^{-9} \text{ m}^4 \cdot \text{MPa}^{-1} \cdot \text{s}^{-1}$  at  $20 \text{ }^\circ\text{C}$ ),  $\rho$  is the density of  
 297 water ( $9.982 \times 10^5 \text{ g} \cdot \text{m}^{-3}$ ) and  $A_x$  is the xylem cross-section area.

298 The pit fraction ( $F_p$ ) was defined as the product of the pit-field fraction ( $F_{pf}$ ) and the contact  
 299 fraction ( $F_c$ ) (equation 9).

$$300 \quad F_p = F_{pf} \times F_c \quad (9)$$

301 The pit fraction was measured on five individual trees for each growth condition.

302 The vessel area ( $A_v$ ) was estimated as the area of a cylinder according to the equation 10.

$$303 \quad A_v = D_v \times L_v \times \pi + 2\pi \left(\frac{D_v}{2}\right)^2 \quad (10)$$

304 It was measured for 7 droughted, 5 control and 5 shaded trees.

305 The pit area per vessel ( $A_p$ ) was calculated as the product of the vessel area  $A_v$  by pit fraction  
 306  $F_p$  (equation 11).

$$307 \quad A_p = A_v \times F_p \quad (11)$$

308 It was measured for 4 droughted, 5 control and 4 shaded individuals.

309 Xylem water potentials at the onset of xylem embolism ( $P_{12}$ ) and at full embolism ( $P_{88}$ ) were  
 310 calculated using equation 12 and 13 respectively (Domec and Gartner 2001), using the  
 311 experimental values of  $P_{50}$  and  $S$  resulting from equation 1.

$$312 \quad P_{12} = P_{50} + \frac{50}{S} \quad (12)$$

$$313 \quad P_{88} = P_{50} - \frac{50}{S} \quad (13)$$

314

### 315 **Measurement of individual vessel vulnerability to embolism using multispectral approach** 316 **combining X-ray microtomography and light microscopy**

317 Two stem segments from droughted plants and two from control plants were sampled and  
 318 prepared in the same condition as for vulnerability to embolism measurements. We used the  
 319 techniques described in Cochard et al. (2015). Segments were shortened underwater at 34 cm

320 long using a razor blade, sealed in liquid paraffin wax in order to prevent dehydration during  
321 the microtomography scans. A first 21 min scan was acquired using a X-ray microtomography  
322 system (Phoenix Nanotom, General Electric, Boston, MA, USA) at the centre of the segment  
323 as described below to reveal the native state of embolism in each shoot. The field-of view was  
324  $7.8 \times 7.8 \times 7.8 \text{ mm}^3$  and covered each full cross section of the samples. X-ray source settings  
325 were 60 kV and 240  $\mu\text{A}$ . 1000 images were recorded during the  $360^\circ$  rotation of the sample  
326 and the final spatial resolution was 3.9  $\mu\text{m}$ .

327 Then, the paraffin was broken at the ends in order to allow the water flow and the sample was  
328 set in a Cavitron during 5 min at 0.8 MPa, immersed in paraffin and scanned again with the X-  
329 ray microtomograph at the same location than previously in order to observe the new embolism  
330 status. The same procedure was repeated for increasing pressure steps, until - 4 MPa (Fig. 1).

331 Then, the stem sample was cut in the air at 5 mm above the scanned section in order to generate  
332 100 % of embolism of the functional vessels and a last microtomographic scan was performed  
333 in order to visualize this complete vessel network.

334 The sample was then dried several days in room conditions and a transverse section of 25  $\mu\text{m}$   
335 thick was cut with a rotary microtome (RM2165, Leica Microsystems). Sections were dyed  
336 with series of baths as following: bleach (about 15 sec), acetic acid, Astra blue (1 min), acetic  
337 acid, safranin (1 min), acetic acid with a water bath between each solution, then an ethanol  
338 series (50, 70, 100 and 100 %). The sections were mounted in Eukitt. Images were processed  
339 using a microscope (Zeiss Axio Observer Z1), a digital camera (AxioCam MRc) and Zen  
340 imaging software system (Zeiss, Jena, Germany). Image analyses were performed using Fiji  
341 software (under ImageJ version 2.0.0-rc-68/1.52h) (Schindelin et al. 2012, Schneider et al.  
342 2012), using the same method described in the section for light microscopy. The diameter of  
343 each vessel ( $D_v^*$ ) was estimated as the diameter of the circle that provided the same area as the  
344 vessel lumen. For each vessel, the number of vessels in the group (Group Size; GS) and the

345 fraction of membrane in contact with other vessels ( $F_c^*$ ) were also estimated on the cross-  
346 section plane. Finally, the relative distance from the pith was measured for each vessel as the  
347 ratio of the distance from the pith to the vessel over the distance from the pith to the cambium.  
348 The microtomography scans were reconstructed in three-dimension (3D) using Phoenix datosx  
349 2 software (General Electric, Boston, MA, USA) with spatial resolution of  $6.8 \times 6.8 \times 6.8 \mu\text{m}^3$   
350 per voxel. Then, for each 3D-reconstruction, a cross section was extracted at the exact same  
351 location as with the microscopy section. For each vessel in the cross sections, its embolism  
352 pressure ( $P_e$ ) is defined as being the centrifugation-induced pressure from which the vessel  
353 appeared to be air-filled on microtomographic images (Fig. 1, A-D).

354 For each sample, images from x-ray microtomography observation (virtual cross sections built  
355 by 3D reconstruction) were aligned on the light microscopy image (stem cross section observed  
356 by light microscopy) using the “Align image by line ROI” tool (Schindelin et al. 2012) of Fiji  
357 software. A unique identification number was given to each vessel observed in images from  
358 both techniques, in order to link the embolism pressure with anatomical parameters (Fig. 1, E).  
359 A total of 2570 vessels were identified. Vessels were grouped per  $D_v^*$ , per  $F_c^*$  and per GS  
360 classes. Classes were sized to be as uniform as possible, counting from 183 up to 748 vessels.  
361 A total of 1100 solitary vessels were grouped in the same class when required. Cumulative  
362 number of embolized vessels was plotted according to their  $P_e$  and, for each class, a Weibull  
363 function was fit (equation 1).

#### 364 **Statistical analysis**

365 The statistical analysis was performed using the RStudio software (version 1.1.456; running  
366 under R core version 3.5.1, R Development Core Team 2008). One way ANOVA was used for  
367 comparing the means between the three growth conditions. When we found a significant  
368 difference, we referred to Tukey’s multiple range test at  $p < 0.05$  to compare the mean values



369 between growth conditions. The correlations between the structural traits and the  $P_{50}$  and  $P_e$   
370 were calculated using linear regressions.

371

## 372 **Results**

373 Continuous recordings of the radial growth showed a significant lower growth for the droughted  
374 plants throughout the experiment (Fig. S2, Table 2). These plants also showed a lower height,  
375 lower leaf area, lower  $\Psi_{pd}$  and lower  $\Psi_{md}$ , demonstrating the significant effect of our drought  
376 treatment. The higher leaf area for shaded plants compared to control plants is an evidence that  
377 the shading conditions affected the plant development.

378 Growing plants under different environmental conditions aimed to induce wide variations in  
379 xylem vulnerability to embolism. The three growth conditions spread the measured  $P_{50}$  over  
380 range from - 2.00 to - 3.47 MPa (Table S1), with a difference of 1.04 MPa between the most  
381 resistant droughted plant and the most vulnerable control plant and a difference of 1.47 MPa  
382 between the most resistant droughted plant and the most vulnerable shaded plant. A  
383 significantly lower  $P_{50}$  was found on droughted plants when compared to control and shaded  
384 plants ( $p < 0.001$ , Table 2), while the slopes of the vulnerability curves were not different  
385 between the growth conditions (Fig. 2, A). Despite a slightly higher native embolism for  
386 droughted plants compared to shaded plants,  $\Psi_{mid}$  was higher than the inflexion point of the  
387 vulnerability curve ( $P_{12}$ ) for every growth conditions. This allows excluding any effect of these  
388 quite low native embolism on measured  $P_{50}$ . We observed no difference for mean  $K_S$  between  
389 the growth conditions (Fig. 2, B), suggesting no plasticity for this trait in our experimental  
390 conditions. When considering the vessel diameter, a reduced  $K_{S\_theo}$  was measured in the  
391 droughted plants compared to control and shaded plants (Table 2).

392 The analyses combining different methods (light microscopy, TEM, SEM), allowed measuring  
 393 a large set of anatomical traits from tissue to pit levels. The correlation between these traits and  
 394 the  $P_{50}$  was assessed (Fig. 3, 4).

395 The traits measured at tissue level (GI, SI and  $F_p$ ) showed a strong linear correlation with  $P_{50}$   
 396 ( $R^2 > 0.70$ ;  $p < 0.001$ ; Fig. 3, 4), except  $F_c$  that exhibited a weaker correlation ( $R^2 = 0.38$ ;  $p =$   
 397  $0.004$ ). These results put in light a relationship between vessel connectivity, vessel grouping  
 398 and vulnerability to embolism (negative relationship for  $F_c$ , GI and  $F_p$ ; positive relationship for  
 399 SI). However, we found no correlation between pit-field fraction ( $F_{pf}$ ) and  $P_{50}$ , with no variation  
 400 among the growth conditions (Table 3). We observed a strong positive relationship ( $p < 0.001$ )  
 401 between  $P_{50}$  and the vessel dimensions ( $L_v$ ,  $D_v$  and  $A_v$ ) showing that larger vessels with larger  
 402 pit area tend to be associated with an increase in vulnerability to embolism ( $R^2 > 0.75$ ;  
 403  $p < 0.001$ ). The positive correlation between  $P_{50}$  and  $A_p$  ( $R^2 = 0.78$ ;  $p < 0.001$ , Fig. 4)  
 404 highlighted the link between the area of vessels covered by bordered pits and the xylem  
 405 vulnerability to embolism.

406 No linear correlation appeared between the pit structure parameters ( $D_a$ ,  $D_p$ ,  $L_p$  and  $T_m$ ) and the  
 407  $P_{50}$ : we observed no variation for  $D_a$ ,  $D_p$  and  $T_m$  among growth conditions.

408 Using x-ray microtomograph, the direct visualization of embolism inside the xylem (Fig. 1)  
 409 allowed evaluating the vulnerability to embolism ( $P_e$ ) of individual vessels. The multispectral  
 410 analysis combining x-ray tomographic observations and the measurements made on light  
 411 microscopy images allowed establishing the link between  $P_e$  and the structural parameters of  
 412 each vessel (Fig. 5). The correlation between  $D_v^*$  and  $P_e$  (Fig. 5, A) was clear: wider vessels  
 413 appeared more vulnerable than the narrower ones.  $F_c^*$  showed a smaller influence on  $P_e$  (Fig.  
 414 5, B): solitary vessels ( $F_c^* \leq 1\%$ ) and weakly connected vessels ( $1 < F_c^* \leq 20\%$ ) were more  
 415 vulnerable than the highly connected vessels ( $F_c^* > 20\%$ ). The link between GS and  $P_e$  (Fig. 5,  
 416 C) appeared to be the less clear: the most vulnerable vessels were the solitary ones whereas the

417 grouped vessels ( $GS \geq 2$ ) were less vulnerable. Despite a significant correlation between  $P_e$   
418 and  $D_v^*$ ,  $F_c^*$  and GS ( $p < 0.001$ ; Fig. 6), the strength of the correlation was poor ( $R^2 < 0.25$ ).  
419 We also noticed that the position of the vessel in the cross section is linked to its vulnerability  
420 (Fig 1): the more the vessels were far from the pith, the more they were more resistant to  
421 embolism. ( $R^2 = 0.49$ ;  $p < 0.001$ ; Fig. 5, D; Fig. 6).

422

## 423 Discussion

424 The range for  $P_{50}$  plasticity induced by the growth conditions was large: 0.76 MPa between the  
425 mean  $P_{50}$  of droughted and shaded plants (Table 2; Fig. 2, A) and up to 1.47 MPa between two  
426 individuals. This is consistent with previous studies: Awad et al. (2010) reported a difference  
427 of 0.63 MPa between droughted and well-watered plants; Plavcová and Hacke (2012) reported  
428 a difference of 1.08 MPa between droughted and shaded *Populus trichocarpa x deltoides* plants.  
429 Therefore, the plasticity induced by our experimental setup was probably close to the maximum  
430 we could expect according to the literature.

431 The absence of difference in specific hydraulic conductivity ( $K_s$ ) between droughted and control  
432 plants (Table 2; Fig. 2, B) was consistent with the results of Gleason et al. (2016): who reported  
433 a poor correlation between vulnerability to embolism and  $K_s$  in their meta-analysis.  
434 Furthermore, the lack of trade-off between hydraulic efficiency and safety was also observed  
435 within species (Awad et al. 2010, Plavcová and Hacke 2012, Schuldt et al. 2016). A significant  
436 decrease of the theoretical conductivities ( $K_{s\_theo}$ ) was found for droughted plants compared to  
437 other plants (Table 2), relying on a decrease in vessel diameter ( $D_v$ ) (Table 3); whereas the pit  
438 structure was not modified (Table 3). However, This theoretical decrease in lumen conductance  
439 in droughted plants is only based on the Poiseuille's law and could be offset by other changes  
440 we did not investigate, such as three-dimensional xylem organization, vessel wall sculpturing,  
441 pit biochemistry or pit membrane porosity.

442  $P_{50}$  was correlated with anatomical traits related to pit quantity characteristics measured at the  
443 xylem and vessel levels (significant correlations with  $R^2 > 0.7$  for 7 out of the 9 traits; Fig. 3,  
444 4). These pit quantity parameters were correlated between them, which is not very surprising  
445 since they all measure slightly different features of vessel connectivity (Table S2; Fig. S3).  
446 Indeed, such correlations were also found when comparing *Acer* species (Lens et al. 2011). By  
447 contrast, no correlation was found with the traits related to the pit dimensions ( $D_a$ ,  $D_p$ ,  $L_p$  and  
448  $T_m$ ; Fig. 3). Thus, the pit ultrastructure does not appear as a driver of the plasticity of  
449 vulnerability to embolism in *Populus tremula x alba* (Fig. S1). Despite a key role of  $T_m$  in  
450 determining vulnerability to embolism, the air-seeding pressures for thin pit membrane such as  
451 those of poplar xylem would not be influenced by slight changes in its thickness (Li et al. 2016,  
452 Kaack et al. 2019). So, the role of pit structure in plasticity of vulnerability to embolism remains  
453 to be tested in species having much thicker intervessel pit membranes. The observation of a  
454 variation in vessel diameter not associated with a variation in pit membrane thickness is not  
455 surprising, since this has already been reported when comparing the anatomy between organs  
456 along the flow path in several species of angiosperm (Klepsch et al. 2018). Other relevant pit  
457 parameters could also be considered, but suitable methods for investigating their variability are  
458 lacking. For example, the pit membrane porosity contributes to the differences in vulnerability  
459 to embolism (Jansen et al. 2009, Li et al. 2016, Kaack et al. 2019); but this parameter is difficult  
460 to measure accurately because pores include a series of various pore constrictions, and the  
461 narrowest constriction should be the main bottleneck (Kaack et al. 2019, Kaack et al. 2020,  
462 Zhang et al. 2020). The role of the biochemical composition of the pit membrane in the  
463 plasticity of vulnerability to embolism cannot be excluded too. Besides, there have been recent  
464 advances in the understanding of the pit membrane biochemistry, including a role for lipids  
465 (Herbette et al. 2015, Klepsch et al. 2016, Schenk et al. 2017, Pereira et al. 2018, Schenk et al.  
466 2018, Kaack et al. 2019). Moreover, calcium in pit membrane was reported to be a major

467 determinant of between-species differences in vulnerability to embolism, but it was not  
468 involved in the plasticity of vulnerability to embolism (Herbette and Cochard 2010).

469 At the interspecific level, pit ultrastructure parameters, especially the pit membrane thickness,  
470 was identified as the major traits involved in variation in vulnerability to embolism (Jansen et  
471 al. 2009; Tixier et al. 2014, Li et al. 2016, Kaack et al. 2019). In addition, between species  
472 differences in vulnerability to embolism also depend on pit mechanical behaviour (Tixier et al.  
473 2014). The probability for air seeding through large pores is expected to be higher when more  
474 pits are present (rare pit hypothesis proposed by Christman et al. 2009). The pit area can thus  
475 explain differences in vulnerability to embolism for some angiosperm groups but not for others  
476 (Lens et al. 2013). Thus, when explaining the variability in vulnerability to embolism between  
477 species, this trait, which depends on the vessel dimensions and xylem organization, does not  
478 appear very relevant (Lens et al. 2013). Lens et al. (2011) tested the relationship between several  
479 pit quantity and pit structure properties and vulnerability to embolism for 11 acer species. They  
480 found that vulnerability to embolism strongly correlated with depth of bordered pit chamber  
481 ( $L_p$ ) and pit membrane thickness ( $T_m$ ) whereas no relationship was found between vulnerability  
482 to embolism and vessel diameter ( $D_v$ ) and total pit area per vessel ( $A_p$ ). By contrast, our results  
483 suggest that the plasticity of vulnerability to embolism in poplar is controlled by the xylem  
484 organization and vessel dimensions, and not by changes in pit structure. Thus, the mechanisms  
485 controlling the inter-specific variability in vulnerability to embolism seem to be different from  
486 the drivers of the within species plasticity in poplar. Complementary works on plasticity need  
487 to be carried out on other species, particularly on species with much thicker pit membranes, in  
488 order to test the genericity of the findings of this study. It would not be surprising if the  
489 mechanisms of plasticity could be different depending on the species. A recent modelling  
490 analysis of the relationships between the functional and structural pit properties provides some  
491 interesting insights agreeing with our results and supporting different mechanisms for plasticity

492 (Kaack et al. 2020). According to this analysis considering the internal structure of the pit  
493 membrane, three functional types of pit can be distinguished based on their  $T_m$ : (1) a pit with a  
494 thin  $T_m$  ( $< 150$  nm) would have large pores causing a low embolism resistance not very sensitive  
495 to the pit area, (2) a pit with a thick  $T_m$  ( $>400$  nm) with narrow pores allowing high embolism  
496 resistance insensitive to the pit area and (3) an intermediate pit membrane type, with embolism  
497 resistance strongly affected by the pit area. This latter type includes the case we studied and  
498 thus it agrees well with our results. Indeed, the model predicts that the vulnerability to embolism  
499 is strongly affected by the pit area for vessels with a pit membrane thickness of 250 nm.

500 The multispectral analysis combining X-ray microtomography analysis with light microscopy  
501 revealed that  $P_e$  shows the strongest correlation with the position of the vessel relative to the  
502 pith (Fig. 6). However, significant correlations were also found between the others xylem traits  
503 ( $D_v$ ,  $F_c$  and GS) and this radial position ( $p < 0.001$ ), so no clear conclusion can be drawn about  
504 an effect of vessel age or position on its vulnerability to embolism. The stem fully developed  
505 in 3 months, and much less for the secondary xylem of the stem part investigated by X-ray  
506 microtomography. We thus assume that the age difference is too weak to explain such  
507 difference in vulnerability to embolism. Indeed, in diffuse-porous species, an age effect in  
508 vulnerability to embolism has been reported between vessels formed in different years but not  
509 between vessels of the same year (Melcher et al. 2003). Moreover, investigations of the  
510 embolism spread in current-year stem of vine or walnut tree using the same approach did not  
511 conclude to an age effect in the secondary xylem (Brodersen et al. 2013, Knipfer et al. 2015).  
512 These two previous studies showed that embolisms formed first in vessels surrounding the pith,  
513 then they spreaded overwhelmingly radially while the water potential was decreasing. The  
514 sequence of embolism formation and spreading in our study could therefore be related to the  
515 mechanism explained by Brodersen et al. (2013). More, we also hypothesize that vulnerability  
516 to embolism decreased during development in relation to changing water conditions *in planta*.

517 Although the soil moisture content was kept constant, the midday water potential of the plant  
518 decreased as the plant grew (Table 2). The pressure inducing embolism being correlated with  
519 the midday water potential experienced by plants (Awad et al. 2010), the acclimation of  
520 vulnerability to embolism would occur during the development of plants.

521 Vulnerability curves are commonly established by measuring the impact of embolism on the  
522 conductance, but not the embolism rates. Thus, “hydraulic vulnerability” is a more suitable term  
523 when comparing xylems for  $P_{50}$  using these methods. Conversely, X-ray microtomography  
524 methods really allow assessing the local vulnerability to embolism.

525 Our results showing a strong relationship between  $P_{50}$  and some vessel and xylem tissue  
526 parameters provide three non-exclusive explanations for the acclimation of hydraulic  
527 vulnerability. This latter relies on changes in vulnerability to embolism of the vessels or on  
528 changes in the effect of the embolism on conductance. First, our study shows that vulnerable  
529 individuals exhibited larger vessels (both longer ( $L_v$ ) and wider ( $D_v$ ); Fig. 3). When a large  
530 vessel embolizes, it generates a greater impact on the hydraulic conductivity compared to a  
531 smaller vessel. Thus, a xylem having a high proportion of large vessels undergoes an important  
532 drop of conductivity after each vessel embolism. Second, we found that vulnerable xylems had  
533 a greater SI and a lower GI and  $F_c$ . Redundancy in the xylem has already been linked with a  
534 lower hydraulic vulnerability using a modelling approach (Ewers et al. 2007, Mrad et al. 2018).  
535 High connectivity and grouping is an efficient way to maintain the hydraulic conductance  
536 despite embolized vessels in the xylem by providing alternative pathways to the water flow  
537 (Carlquist 1966, Schuldt et al. 2016). Third, larger vessels have a larger pit area per vessel ( $A_p$ )  
538 and would thus be more prone to embolism, according to the pit area hypothesis (Christman et  
539 al. 2009). Multispectral analysis combining X-ray microtomography and light microscopy  
540 allowed monitoring the dynamics of xylem embolism and in particular determining the  
541 embolism pressure of each vessel (Fig.1; Fig. 5). This approach supports the third explanation,

542 since larger vessels ( $D_v^*$ ) showed a higher vulnerability to embolism— as noticed by Cai and  
543 Tyree (2010) using a statistical, indirect and destructive technique and by Jacobsen et al. (2019)  
544 using a similar approach. Nevertheless, the poor correlations (low  $R^2$  values) between the  
545 embolism pressure of each vessel ( $P_e$ ) and  $D_v^*$ ,  $F_c^*$  or GS suggest that the rare pit hypothesis is  
546 far from being sufficient for explaining the hydraulic vulnerability inside a stem sample.  
547 According to Kaack et al. (2019), the rare pit hypothesis is not compatible with the three  
548 dimensional structure of the pit. Other additional mechanisms could be involved to explain the  
549 plasticity of hydraulic vulnerability observed among growth conditions: they would include the  
550 effect of redundancy and of vessel embolized volume on the loss of conductance, or change in  
551 pore constrictions in pit membranes. That is why we assume that the different mechanisms we  
552 described here act together to design the hydraulic vulnerability during acclimation. The lowest  
553 correlations found between  $P_e$  and  $F_c^*$  or GS point to the limitations of a bi-dimensional  
554 approach to analyse vessel connectivity. Some studies reported analyses of the three-  
555 dimensional xylem network (Brodersen et al. 2011), that allowed investigating events of  
556 embolism formation and spreading (Brodersen et al. 2013, Knipfer et al. 2015, 2016, Torres et  
557 al. 2016). Rather short segments (2-6 mm long) were examined what was enough for their study.  
558 The vessels having an average length of about ten cm (up to 30 cm), would require analysis of  
559 the vessel organization over a longer sample length for a full quantification of their  
560 connectivity. This was impossible with the x-ray microtomograph device we used. Moreover,  
561 such a large volume of wood could not be scanned without a very high temperature increase to  
562 maintain sufficient resolution.

563 In conclusion, we found that the acclimation of vulnerability to embolism to contrasted growth  
564 conditions in hybrid poplar did not rely on a change in pit ultrastructure, contrary to what was  
565 reported when comparing species. Thus, within-species plasticity in hybrid poplar and between-  
566 species variability for vulnerability to embolism could rely on different mechanisms. We



567 showed that an increase in resistance to embolism in poplar is related to an increase in vessels  
568 connectivity and grouping and a decrease in vessel dimensions, leading to reduce the likelihood  
569 of air seeding through a pit and the effect the resulting embolism events on hydraulic  
570 conductance. This study will allow focusing on the relevant candidate genes controlling  
571 vulnerability to embolism such as those involved in vessels grouping and connectivity or vessel  
572 dimensions. These genes include the aquaporins involved in cell expansion during xylogenesis  
573 (Plavcová et al. 2013), the genes controlling the cell wall metabolism in xylem such as *VND6*,  
574 *VND7* and *MYB46*, which expression levels changed in response to an abiotic stress (Plavcová  
575 et al. 2013, Taylor-Teeples et al. 2016) or *CLE* genes (*CLE41* and *CLE44*) that repress the  
576 xylem differentiation (De Rybel et al. 2016).

577

#### 578 **Funding**

579 This work was supported by European Union within the context of European Regional  
580 Development Fund (ERDF).

#### 581 **Acknowledgements**

582 The authors thank Christelle Boisselet and Brigitte Girard for the plant production, Christophe  
583 Serre for the LDVT preparation, Romain Souchal for the balances and LVDT set up, Patrice  
584 Chaleil, Aline Faure and Stephane Ploquin for growing the plants in the greenhouse, André  
585 Marquier for the PAR measurements and Felix Hartmann for his help in calculating the vessel  
586 length. The authors also thank the PhenoBois platform for the X-ray microtomography facility.

#### 587 **Authors' contributions**

588 C.L. and S.H. designed the study and wrote the manuscript with contributions from all authors.  
589 C.L., S.H., P.C. and J.C. performed field work and hydraulic measurements; C.L., N.B-M.,  
590 Y.Q., L.B. and J.S. performed electron microscopy; C.L., N.B-M., P.C. performed light

591 microscopy; C.L., P.C. and E.B. performed X-ray microCT; C.L., P.C. and E.B. performed  
592 image analysis. All authors approved this manuscript.

593 **References**

- 594 Adams HD, Zeppel MJB, Anderegg WRL, Hartmann H, Landhäusser SM, Tissue DT, Huxman  
595 TE, Hudson PJ, Franz TE, Allen CD, Anderegg LDL, Barron-Gafford GA, Beerling DJ,  
596 Breshears DD, Brodribb TJ, Bugmann H, Cobb RC, Collins AD, Dickman LT, Duan H,  
597 Ewers BE, Galiano L, Galvez DA, Garcia-Forner N, Gaylord ML, Germino MJ, Gessler  
598 A, Hacke UG, Hakamada R, Hector A, Jenkins MW, Kane JM, Kolb TE, Law DJ, Lewis  
599 JD, Limousin J-M, Love DM, Macalady AK, Martínez-Vilalta J, Mencuccini M,  
600 Mitchell PJ, Muss JD, O'Brien MJ, O'Grady AP, Pangle RE, Pinkard EA, Piper FI,  
601 Plaut JA, Pockman WT, Quirk J, Reinhardt K, Ripullone F, Ryan MG, Sala A, Sevanto  
602 S, Sperry JS, Vargas R, Vennetier M, Way DA, Xu C, Yezpez EA, McDowell NG (2017)  
603 A multi-species synthesis of physiological mechanisms in drought-induced tree  
604 mortality. *Nat Ecol Evol* 1:1285–1291.
- 605 Allario T, Tixier A, Awad H, Lemaire C, Brunel N, Badel É, Barigah TS, Julien J-L, Peyret P,  
606 Mellerowicz EJ, Cochard H, Herbette S (2018) PtxtPME1 and homogalacturonans  
607 influence xylem hydraulic properties in poplar. *Physiol Plant* 163:502–515.
- 608 Anderegg WRL, Flint A, Huang C, Flint L, Berry JA, Davis FW, Sperry JS, Field CB (2015)  
609 Tree mortality predicted from drought-induced vascular damage. *Nature Geosci* 8:367–  
610 371.
- 611 Anderegg WRL, Klein T, Bartlett M, Sack L, Pellegrini AFA, Choat B, Jansen S (2016) Meta-  
612 analysis reveals that hydraulic traits explain cross-species patterns of drought-induced  
613 tree mortality across the globe. *PNAS* 113:5024–5029.
- 614 Awad H, Barigah T, Badel É, Cochard H, Herbette S (2010) Poplar vulnerability to xylem  
615 cavitation acclimates to drier soil conditions. *Physiol Plant* 139:280–288.
- 616 Barigah TS, Charrier O, Douris M, Bonhomme M, Herbette S, Améglio T, Fichot R, Brignolas  
617 F, Cochard H (2013) Water stress-induced xylem hydraulic failure is a causal factor of  
618 tree mortality in beech and poplar. *Ann Bot* 112:1431–1437.
- 619 Barigah TS, Ibrahim T, Bogard A, Faivre-Vuillin B, Lagneau LA, Montpied P, Dreyer E (2006)  
620 Irradiance-induced plasticity in the hydraulic properties of saplings of different  
621 temperate broad-leaved forest tree species. *Tree Physiol* 26:1505–1516.
- 622 Brodersen CR, Lee EF, Choat B, Jansen S, Phillips RJ, Shackel KA, McElrone AJ, Matthews  
623 MA (2011) Automated analysis of three-dimensional xylem networks using high-  
624 resolution computed tomography. *New Phytol* 191(4), 1168–1179.
- 625 Brodersen CR, McElrone AJ, Choat B, Lee EF, Shackel KA, Matthews MA (2013) In vivo  
626 visualizations of drought-induced embolism spread in *Vitis vinifera*. *Plant Physiol*  
627 161(4): 1820–1829.
- 628 Cai J, Tyree MT (2010) The impact of vessel size on vulnerability curves: data and models for  
629 within-species variability in saplings of aspen, *Populus tremuloides* Michx. *Plant Cell*  
630 *Env* 33:1059–1069.
- 631 Carlquist S (1966) Wood Anatomy of Compositae: A Summary, With Comments on Factors  
632 Controlling Wood Evolution. *Aliso: A Journal of Systematic and Evolutionary Botany*  
633 6:25–44.

- 634 Choat B, Cobb AR, Jansen S (2008) Structure and function of bordered pits: new discoveries  
635 and impacts on whole-plant hydraulic function. *New Phytol* 177: 608–626.
- 636 Choat B, Jansen S, Brodribb TJ, Cochard H, Delzon S, Bhaskar R, Bucci SJ, Feild TS, Gleason  
637 SM, Hacke UG, Jacobsen AL, Lens F, Maherali H, Martínez-Vilalta J, Mayr S,  
638 Mencuccini M, Mitchell PJ, Nardini A, Pittermann J, Pratt RB, Sperry JS, Westoby M,  
639 Wright IJ, Zanne AE (2012) Global convergence in the vulnerability of forests to  
640 drought. *Nature* 491:752–755.
- 641 Choat B, Pittermann J (2009) New insights into bordered pit structure and cavitation resistance  
642 in angiosperms and conifers. *New Phytol* 182: 557–560.
- 643 Christman MA, Sperry JS, Adler FR (2009) Testing the ‘rare pit’ hypothesis for xylem  
644 cavitation resistance in three species of *Acer*. *New Phytol* 182:664–674.
- 645 Cochard H (2002) A technique for measuring xylem hydraulic conductance under high negative  
646 pressures. *Plant Cell Env* 25:815–819.
- 647 Cochard H, Badel E, Herbette S, Delzon S, Choat B, Jansen S (2013) Methods for measuring  
648 plant vulnerability to cavitation: a critical review. *J Exp Bot* 64:4779–4791.
- 649 Cochard H, Damour G, Bodet C, Tharwat I, Poirier M, Améglio T (2005) Evaluation of a new  
650 centrifuge technique for rapid generation of xylem vulnerability curves. *Physiol Plant*  
651 124:410–418.
- 652 Cochard H, Delzon S, Badel É (2015) X-ray microtomography (micro-CT): a reference  
653 technology for high-resolution quantification of xylem embolism in trees. *Plant Cell*  
654 *Env* 38:201–206.
- 655 Cochard H, Hölttä T, Herbette S, Delzon S, Mencuccini M (2009) New insights into the  
656 mechanisms of water-stress-induced cavitation in conifers. *Plant Physiol* 151:949–954.
- 657 Cohen S, Bennink J, Tyree M (2003) Air method measurements of apple vessel length  
658 distributions with improved apparatus and theory. *J Exp Bot* 54:1889–1897.
- 659 Cooke JEK, Martin TA, Davis JM (2005) Short-term physiological and developmental  
660 responses to nitrogen availability in hybrid poplar. *New Phytol* 167:41–52.
- 661 De Rybel B, Mähönen AP, Helariutta Y, Weijers D (2016) Plant vascular development: from  
662 early specification to differentiation. *Nat Rev Mol Cell Biol* 17:30–40.
- 663 Domec J-C, Gartner BL (2001) Cavitation and water storage capacity in bole xylem segments  
664 of mature and young Douglas-fir trees. *Trees* 15:204–214.
- 665 Ewers FW, Ewers JM, Jacobsen AL, López-Portillo J (2007) Vessel redundancy: Modeling  
666 safety in numbers. *IAWA J* 28:373–388.
- 667 Fichot R, Barigah TS, Chamaillard S, Le Thiec D, Laurans F, Cochard H, Brignolas F (2010)  
668 Common trade-offs between xylem resistance to cavitation and other physiological  
669 traits do not hold among unrelated *Populus deltoides* × *Populus nigra* hybrids. *Plant Cell*  
670 *Env* 33:1553–1568.

- 671 Gleason SM, Westoby M, Jansen S, Choat B, Hacke UG, Pratt RB, Bhaskar R, Brodribb TJ,  
672 Bucci SJ, Cao K-F, Cochard H, Delzon S, Domec J-C, Fan Z-X, Feild TS, Jacobsen AL,  
673 Johnson DM, Lens F, Maherali H, Martínez-Vilalta J, Mayr S, McCulloh KA,  
674 Mencuccini M, Mitchell PJ, Morris H, Nardini A, Pittermann J, Plavcová L, Schreiber  
675 SG, Sperry JS, Wright IJ, Zanne AE (2016) Weak tradeoff between xylem safety and  
676 xylem-specific hydraulic efficiency across the world's woody plant species. *New Phytol*  
677 209:123–136.
- 678 Hacke UG, Sperry JS, Wheeler JK, Castro L (2006) Scaling of angiosperm xylem structure  
679 with safety and efficiency. *Tree Physiol* 26: 689–701.
- 680 Hajek P, Leuschner C, Hertel D, Delzon S, Schuldt B (2014) Trade-offs between xylem  
681 hydraulic properties, wood anatomy and yield in *Populus*. *Tree Physiol* 34:744–756.
- 682 Hammond WM, Yu K, Wilson LA, Will RE, Anderegg WRL, Adams HD (2019) Dead or  
683 dying? Quantifying the point of no return from hydraulic failure in drought-induced tree  
684 mortality. *New Phytol* 223:1834–1843.
- 685 Hartmann H, McDowell NG, Trumbore S (2015) Allocation to carbon storage pools in Norway  
686 spruce saplings under drought and low CO<sub>2</sub>. *Tree Physiol* 35:243–252.
- 687 Herbette S, Bouchet B, Brunel N, Bonnin E, Cochard H, Guillon F (2015) Immunolabelling of  
688 intervessel pits for polysaccharides and lignin helps in understanding their hydraulic  
689 properties in *Populus tremula* × *alba*. *Ann Bot* 115:187–199.
- 690 Herbette S, Cochard H (2010) Calcium Is a Major Determinant of Xylem Vulnerability to  
691 Cavitation. *Plant Physiol* 153:1932–1939.
- 692 Herbette S, Wortemann R, Awad H, Huc R, Cochard H, Barigah TS (2010) Insights into xylem  
693 vulnerability to cavitation in *Fagus sylvatica* L.: phenotypic and environmental sources  
694 of variability. *Tree Physiol* 30:1448–1455.
- 695 Jacobsen AL, Pratt RB, Venturas MD, Hacke UG (2019) Large volume vessels are vulnerable  
696 to water-stress-induced embolism in stems of poplar. *IAWA J* 40: 4-22.
- 697 Jansen S, Klepsch M, Li S, Kotowska M, Schiele S, Zhang Y, Schenk H (2018) Challenges in  
698 understanding air-seeding in angiosperm xylem. *Acta Hort* 1222: 13-20.
- 699 Jansen S, Choat B, Pletsers A (2009) Morphological variation of intervessel pit membranes and  
700 implications to xylem function in angiosperms. *Am J Bot* 96:409–419.
- 701 Jinagool W, Lamacque L, Delmas M, Delzon S, Cochard H, Herbette S (2018) Is there  
702 variability for xylem vulnerability to cavitation in walnut tree cultivars and species  
703 (*Juglans* spp.)? *HortSci* 53:132–137.
- 704 Jinagool W, Rattanawong R, Sangsing K, Barigah TS, Gay F, Cochard H, Kasemsap P,  
705 Herbette S (2015) Clonal variability for vulnerability to cavitation and other drought-  
706 related traits in *Hevea brasiliensis* Müll. Arg. *J Plant Hydraul* 2:e001.
- 707 Kaack L, Altaner CM, Carmesin C, Diaz A, Holler M, Kranz C, Neusser G, Odstrcil M, Schenk  
708 HJ, Schmidt V, Weber M, Zhang Y, Jansen S (2019) Function and three-dimensional  
709 structure of intervessel pit membranes in angiosperms: a review. *IAWA J* 40:673–702.

- 710 Kaack L, Weber M, Isasa E, Karimi Z, Li S, Pereira L, Trabi CL, Zhang Y, Schenk HJ, Schuldt  
711 B, Schmidt V, Jansen S (2020) Pore constrictions in intervessel pit membranes reduce  
712 the risk of embolism spreading in angiosperm xylem. *bioRxiv*:345413.
- 713 Klepsch MM, Schmitt M, Paul Knox J, Jansen S (2016) The chemical identity of intervessel pit  
714 membranes in *Acer* challenges hydrogel control of xylem hydraulic conductivity. *AoB*  
715 *PLANTS* 8: plw052.
- 716 Klepsch M, Zhang Y, Kotowska MM, Lamarque LJ, Nolf M, Schuldt B, Torres-Ruiz JM, Qin  
717 D-W, Choat B, Delzon S, Scoffoni C, Cao K-F, Jansen S (2018) Is xylem of angiosperm  
718 leaves less resistant to embolism than branches? Insights from microCT, hydraulics, and  
719 anatomy. *J Exp Bot* 69:5611–5623.
- 720 Knipfer T, Brodersen CR, Zedan A, Kluepfel DA, McElrone AJ (2015) Patterns of drought-  
721 induced embolism formation and spread in living walnut saplings visualized using X-  
722 ray microtomography. *Tree Physiol* 35: 744-755.
- 723 Knipfer T, Cuneo IF, Brodersen CR, McElrone AJ (2016) In situ visualization of the dynamics  
724 in xylem embolism formation and removal in the absence of root pressure: a study on  
725 excised grapevine stems. *Plant Physiol* 171(2), 1024-1036.
- 726 Lamy J-B, Bouffier L, Burlett R, Plomion C, Cochard H, Delzon S (2011) Uniform selection  
727 as a primary force reducing population genetic differentiation of cavitation resistance  
728 across a species range. *PLOS ONE* 6:e23476.
- 729 Lamy J-B, Plomion C, Kremer A, Delzon S (2012) QST < FST As a signature of canalization.  
730 *Mol Ecol* 21:5646–5655.
- 731 Lens F, Sperry JS, Christman MA, Choat B, Rabaey D, Jansen S (2011) Testing hypotheses  
732 that link wood anatomy to cavitation resistance and hydraulic conductivity in the genus  
733 *Acer*. *New Phytol* 190:709–723.
- 734 Lens F, Tixier A, Cochard H, Sperry JS, Jansen S, Herbette S (2013) Embolism resistance as a  
735 key mechanism to understand adaptive plant strategies. *Cur Op Plant Biol* 16:287–292.
- 736 Li S, Lens F, Espino S, Karimi Z, Klepsch M, Schenk HJ, Schmitt M, Schuldt B, Jansen S  
737 (2016) Intervessel pit membrane thickness as a key determinant of embolism resistance  
738 in angiosperm xylem. *IAWA J* 37:152–171.
- 739 Loepfe L, Martínez-Vilalta J, Pinol J, Mencuccini M (2017) The relevance of the xylem  
740 network structure for plant hydraulic efficiency and safety. *J Th Biol* 247: 788-803.
- 741 Maherali H, Moura CF, Caldeira MC, Willson CJ, Jackson RB (2006) Functional coordination  
742 between leaf gas exchange and vulnerability to xylem cavitation in temperate forest  
743 trees. *Plant Cell Env* 29:571–583.
- 744 Martínez-Vilalta J, Cochard H, Mencuccini M, Sterck F, Herrero A, Korhonen JFJ, Llorens P,  
745 Nikinmaa E, Nolé A, Poyatos R, Ripullone F, Sass-Klaassen U, Zweifel R (2009)  
746 Hydraulic adjustment of Scots pine across Europe. *New Phytol* 184:353–364.
- 747 Melcher PJ, Zwieniecki MA, Holbrook NM (2003) Vulnerability of xylem vessels to cavitation  
748 in sugar maple. Scaling from individual vessels to whole branches. *Plant Physiol* 131(4):

- 749 1775-1780.
- 750 Mrad A, Domec JC, Huang CW, Lens F, Katul G (2018) A network model links wood anatomy  
751 to xylem tissue hydraulic behaviour and vulnerability to cavitation. *Plant Cell Env*  
752 41:2718-2730.
- 753 Niez B, Dlouha J, Moulia B, Badel É (2019) Water-stressed or not, the mechanical acclimation  
754 is a priority requirement for trees. *Trees* 33:279–291.
- 755 Pammenter NW, Van der Willigen C (1998) A mathematical and statistical analysis of the  
756 curves illustrating vulnerability of xylem to cavitation. *Tree Physiol* 18:589–593.
- 757 Pereira L, Flores-Borges DNA, Bittencourt PRL, Mayer JLS, Kiyota E, Araújo P, Jansen S,  
758 Freitas RO, Oliveira RS, Mazzafera P (2018) Infrared nanospectroscopy reveals the  
759 chemical nature of pit membranes in water-conducting cells of the plant xylem. *Plant*  
760 *Physiol* 177:1629–1638.
- 761 Plavcová L, Hacke UG (2012) Phenotypic and developmental plasticity of xylem in hybrid  
762 poplar saplings subjected to experimental drought, nitrogen fertilization, and shading. *J*  
763 *Exp Bot* 63:6481–6491.
- 764 Plavcová L, Hacke UG, Sperry JS (2011) Linking irradiance-induced changes in pit membrane  
765 ultrastructure with xylem vulnerability to cavitation. *Plant Cell Env* 34:501–513.
- 766 Plavcová L, Jansen S, Klepsch M, Hacke UG (2013) Nobody's perfect: can irregularities in pit  
767 structure influence vulnerability to cavitation? *Front Plant Sci* 4: 453.
- 768 Schenk HJ, Espino S, Romo DM, Nima N, Do AYT, Michaud JM, Papahadjopoulos-Sternberg  
769 B, Yang J, Zuo YY, Steppe K, Jansen S (2017) Xylem surfactants introduce a new  
770 element to the cohesion-tension theory. *Plant Physiol* 173:1177–1196.
- 771 Schenk, H. J., Espino, S., Rich-Cavazos, S. M., & Jansen, S. (2018). From the sap's perspective:  
772 the nature of vessel surfaces in angiosperm xylem. *Am J Bot* 105:174-187.
- 773 Schindelin J, Arganda-Carreras I, Frise E, Kaynig V, Longair M, Pietzsch T, Preibisch S,  
774 Rueden C, Saalfeld S, Schmid B, Tinevez J-Y, White DJ, Hartenstein V, Eliceiri K,  
775 Tomancak P, Cardona A (2012) Fiji: an open-source platform for biological-image  
776 analysis. *Nature Methods* 9:676–682.
- 777 Schneider CA, Rasband WS, Eliceiri KW (2012) NIH Image to ImageJ: 25 years of image  
778 analysis. *Nature Methods* 9:671–675.
- 779 Scholander PF, Bradstreet ED, Hemmingsen EA, Hammel HT (1965) Sap pressure in vascular  
780 plants: Negative hydrostatic pressure can be measured in plants. *Sci* 148:339–346.
- 781 Scholz A, Klepsch M, Karimi Z, Jansen S (2013b) How to quantify conduits in wood? *Front*  
782 *Plant Sci* 4:56.
- 783 Scholz A, Rabaey D, Stein A, Cochard H, Smets E, Jansen S (2013a) The evolution and function  
784 of vessel and pit characters with respect to cavitation resistance across 10 *Prunus*  
785 species. *Tree Physiol* 33:684–694.

- 786 Schuldt B, Knutzen F, Delzon S, Jansen S, Müller-Haubold H, Burlett R, Clough Y, Leuschner  
787 C (2016) How adaptable is the hydraulic system of European beech in the face of climate  
788 change-related precipitation reduction? *New Phytol* 210:443–458.
- 789 Sperry JS, Hacke UG, Wheeler JK (2005) Comparative analysis of end wall resistivity in xylem  
790 conduits. *Plant Cell Env* 28:456–465.
- 791 Steudle E (2001) The cohesion-tension mechanism and the acquisition of water by plant roots.  
792 *Ann Rev Plant Physiol Plant Molecul Biol* 52:847–875.
- 793 Taylor-Teeple M, Lin L, Lucas M de, Turco G, Toal TW, Gaudinier A, Young NF, Trabucco  
794 GM, Veling MT, Lamothe R, Handakumbura PP, Xiong G, Wang C, Corwin J,  
795 Tsoukalas A, Zhang L, Ware D, Pauly M, Kliebenstein DJ, Dehesh K, Tagkopoulos I,  
796 Breton G, Pruneda-Paz JL, Ahnert SE, Kay SA, Hazen SP, Brady SM (2015) An  
797 Arabidopsis gene regulatory network for secondary cell wall synthesis. *Nature* 517:571–  
798 575.
- 799 Tixier A, Herbette S, Jansen S, Capron M, Tordjeman P, Cochard H, Badel É (2014) Modelling  
800 the mechanical behaviour of pit membranes in bordered pits with respect to cavitation  
801 resistance in angiosperms. *Ann Bot* 114:325–334.
- 802 Torres-Ruiz J.M., Cochard H., Mencuccini M., Delzon S., Badel E. 2016. Direct observations  
803 and modelling of embolism spread between xylem conduits: a case study in Scot pine.  
804 *Plant Cell Env* 39:2774-2785.
- 805 Tyree MT, Davis SD, Cochard H (1994) Biophysical perspectives of xylem evolution: is there  
806 a tradeoff of hydraulic efficiency for vulnerability to dysfunction? *IAWA J* 15:335–360.
- 807 Wheeler JK, Sperry JS, Hacke UG, Hoang N (2005) Inter-vessel pitting and cavitation in woody  
808 Rosaceae and other vesselled plants: a basis for a safety versus efficiency trade-off in  
809 xylem transport. *Plant Cell Env* 28:800–812.
- 810 Wortemann R, Herbette S, Barigah TS, Fumanal B, Alia R, Ducousso A, Gomory D, Roeckel-  
811 Drevet P, Cochard H (2011) Genotypic variability and phenotypic plasticity of  
812 cavitation resistance in *Fagus sylvatica* L. across Europe. *Tree Physiol* 31:1175–1182.
- 813 Zimmermann MH, Jeje AA (1981) Vessel-length distribution in stems of some American  
814 woody plants. *Can J Bot* 59:1882–1892.
- 815 Zhang Y, Carmesin C, Kaack L, Klepsch MM, Kotowska M, Matei T, Schenk HJ, Weber M,  
816 Walther P, Schmidt V, Jansen S (2020) High porosity with tiny pore constrictions and  
817 unbending pathways characterize the 3D structure of intervessel pit membranes in  
818 angiosperm xylem. *Plant Cell Env* 43:116–130.



819 Figure 1: Measurement of the embolism pressure ( $P_e$ ) of each individual vessel. A-D: Direct  
 820 observation of embolism spread using a x-ray microtomograph in an intact xylem stem under  
 821 increasing tension. Black areas reveal the embolized vessels. A: native state ( $\Psi = 0$  MPa).  
 822 B:  $\Psi = - 1.5$  MPa. C:  $P_{50}$  state ( $\Psi = - 2.5$  MPa). D: final state ( $\Psi = - 4$  MPa). E: Cut of the same  
 823 stem sample observed using light microscopy. The resulting image resolution allows us  
 824 measuring accurately the anatomical traits. Colour represents the embolism pressure ( $P_e$ ) of  
 825 each vessel, as measured with x-ray microtomography. Shown images are from a subset of  
 826 approx. 230 vessels on a control plant.

827

828 Figure 2: Xylem hydraulic traits in trees depending on the growth conditions. A: Xylem  
 829 vulnerability curve. Each line is the mean curve per condition: droughted,  $n = 9$  from 9 trees;  
 830 control,  $n = 10$  from 5 trees; shaded,  $n = 12$  from 6 trees. Dashed line, droughted plants; full  
 831 line, control plants; dotted line, shaded plants. Grey areas represent the standard deviations  
 832 around the means. Horizontal dotted line indicates the 50 % loss of conductance. B: Hydraulic  
 833 specific conductivity ( $K_s$ ). Data are mean values for 8 droughted trees, 9 control trees, 9 shaded  
 834 trees. Error bars show the standard deviation.

835

836 Figure 3: Correlation between  $P_{50}$  and several xylem structural traits. Data are squares of the  
 837 coefficient of correlation ( $R^2$ ) for each factor with  $P_{50}$ . Black bars indicate pit-related traits and  
 838 white bars indicate vessel and xylem-related traits. On the x-axis, a "+" symbol indicates a  
 839 positive correlation, while a "-" symbol indicates a negative one. Stars indicate the significance  
 840 of the correlation: "\*\*\*\*",  $p < 0.001$ ; "\*\*\*",  $0.001 < p < 0.01$ ; "ns", non-significant correlation.

841

842 Figure 4: Correlation between  $P_{50}$  and two xylem structural traits. A: Relationship between  $P_{50}$   
 843 and pit area per vessel ( $A_p$ ). B: Relationship between  $P_{50}$  and vessel grouping index (GI). Each

844 point represents the mean value for an individual tree. Black circles refer to droughted plants;  
845 white circles refer to control plants and white squares refer to shaded plants. The dotted line is  
846 the regression line.

847

848 Figure 5: Correlation between  $P_e$  and vessel traits within xylem. Data are all vessel  
849 measurements pooled from analyses on four individuals using X-ray microtomography. A-C:  
850 Vulnerability to embolism curves of vessels grouped by classes depending on structural traits.  
851 A: Vessels clustered by diameter ( $D_v^*$ ) classes. The dash sizes of the lines indicate the vessel  
852 diameter class: from full line (narrow vessels) to dotted line (wide vessels). B: Vessels clustered  
853 by classes for fraction of membrane length in contact with other vessels ( $F_c^*$ ). The dash sizes  
854 of the lines indicate the vessel contact fraction class: from full line (non-contact vessels) to  
855 dotted line (vessels sharing high portion of membrane length). C: Vessels are clustered by group  
856 size (GS) classes. The dash sizes of the lines indicate the vessel group sizes: from full line  
857 (solitary vessels) to dotted line (vessels in large groups). D: Vessels clustered by distance from  
858 the pith. The relative distance is between 0 and 1, 0 being close to the pith. The dash sizes of  
859 the lines indicate the vessel distance class: from full line (vessels close to the pith) to dotted line  
860 (vessels far from the pith).

861 Figure 6: Correlation between  $P_e$  and xylem traits. Data are squares of the coefficient of  
862 correlation ( $R^2$ ) for each factor with  $P_e$ . On the x-axis, a "+" symbol indicates a positive  
863 correlation, while a "-" symbol indicates a negative one. Stars indicate the significance of the  
864 correlation for the trait: "\*\*\*\*",  $p < 0.001$ .

Table 1: Meanings of the symbols.

<b>Symbol</b>	<b>Definition</b>	<b>Unit</b>
$\Psi_{pd}$	Predawn water potential	MPa
$\Psi_{md}$	Midday water potential	MPa
<b>LA</b>	Mean leaf area	cm <sup>2</sup>
$A_p$	Mean total pit area per vessel	mm <sup>2</sup>
$A_v$	Mean area per vessel	mm <sup>2</sup>
$D_a$	Mean pit aperture diameter	μm
$D_p$	Mean pit diameter	μm
$D_v$	Mean vessel diameter	μm
$D_v^*$	Vessel diameter	μm
$F_c$	Mean contact fraction: mean membrane length in contact with other vessels over total membrane length	%
$F_c^*$	Vessel contact fraction: for each vessel, fraction of membrane length in contact with other vessels	%
$F_p$	Mean pit fraction: mean total pit area in contact with other vessels over total vessel area	%
$F_{pf}$	Mean pit-field fraction: pit area over inter-vessel area	%
<b>GI</b>	Vessel grouping index	-
<b>GS</b>	Vessel group size	-
$K_{s\_theo}$	Theoretical hydraulic conductivity	kg.s <sup>-1</sup> .MPa <sup>-1</sup> .m <sup>-1</sup>
$K_s$	Specific hydraulic conductivity	kg.s <sup>-1</sup> .MPa <sup>-1</sup> .m <sup>-1</sup>
$L_p$	Mean pit chamber depth	μm
$L_v$	Median vessel length	μm
$P_{50}, P_{12}, P_{88}$	Pressure inducing 50, 12, 88 % loss of xylem conductance	MPa
$P_e$	Pressure inducing embolism in a vessel	MPa
<b>SI</b>	Vessel solitary index	%
$T_m$	Mean pit membrane thickness	μm

Table 2: Physiological characterisation of sapling grown under the three different conditions.

Factor	Unit	Droughted	Control	Shaded
$\Psi_{pd}$ m-1	Mpa	- 0.22 ± 0.12 <sup>a</sup>	- 0.11 ± 0.04 <sup>b</sup>	- 0.13 ± 0.01 <sup>b</sup>
$\Psi_{md}$ m-1	MPa	- 0.96 ± 0.15 <sup>a</sup>	- 0.69 ± 0.05 <sup>b</sup>	- 0.77 ± 0.09 <sup>b</sup>
$\Psi_{pd}$ d-1	Mpa	- 0.59 ± 0.44 <sup>a</sup>	- 0.14 ± 0.03 <sup>b</sup>	- 0.11 ± 0.02 <sup>b</sup>
$\Psi_{md}$ d-1	MPa	- 1.44 ± 0.33 <sup>a</sup>	- 0.98 ± 0.06 <sup>b</sup>	- 0.98 ± 0.11 <sup>b</sup>
LA	cm <sup>2</sup>	87.64 ± 18.41 <sup>a</sup>	137.61 ± 17.55 <sup>b</sup>	184.13 ± 40.34 <sup>c</sup>
Height	Mm	1685 ± 187 <sup>a</sup>	2237 ± 263 <sup>b</sup>	2282 ± 76 <sup>b</sup>
Diameter	Mm	9.47 ± 0.83 <sup>a</sup>	13.96 ± 0.49 <sup>b</sup>	10.94 ± 0.61 <sup>b</sup>
$K_{s\_theo}$	kg.s <sup>-1</sup> .MPa <sup>-1</sup> .m <sup>-1</sup>	0.949 ± 0.336 <sup>a</sup>	1.380 ± 0.274 <sup>b</sup>	1.405 ± 0.198 <sup>b</sup>
$K_s$	kg.s <sup>-1</sup> .MPa <sup>-1</sup> .m <sup>-1</sup>	1.054 ± 0.192 <sup>a</sup>	1.043 ± 0.301 <sup>a</sup>	0.954 ± 0.330 <sup>a</sup>
$P_{50}$	MPa	- 3.03 ± 0.23 <sup>a</sup>	- 2.49 ± 0.10 <sup>b</sup>	- 2.27 ± 0.18 <sup>b</sup>
$P_{12}$	MPa	- 2.55 ± 0.34 <sup>a</sup>	- 2.02 ± 0.11 <sup>b</sup>	- 1.87 ± 0.11 <sup>b</sup>
$P_{88}$	MPa	- 3.51 ± 0.24 <sup>a</sup>	- 2.95 ± 0.11 <sup>b</sup>	- 2.68 ± 0.11 <sup>b</sup>
Native Embolism	%	1.81 ± 10.47 <sup>a</sup>	- 7.48 ± 7.91 <sup>ab</sup>	- 10.81 ± 7.84 <sup>b</sup>

Data are mean values ± standard deviation for each growth condition. For each line, values not followed by the same letter differ significantly at  $p < 0.05$  (one-way ANOVA). Water potentials ( $\Psi_{pd}$  and  $\Psi_{md}$ ) were measured one month before (m-1) and the day before (d-1) stem sampling for hydraulic and structural analysis.  $\Psi_{pd}$ , Predawn water potential;  $\Psi_{md}$ , Midday water potential; LA, Leaf area;  $K_{s\_theo}$ , Theoretical hydraulic conductivity;  $K_s$ , Specific hydraulic conductivity;  $P_{50}$ ;  $P_{12}$ ;  $P_{88}$ , pressure inducing 50; 12 and 88 percent loss of conductance.

1 Table 3: Xylem structural traits depending on the growth conditions.

<b>Trait</b>	<b>Unit</b>	<b>Droughted</b>	<b>Control</b>	<b>Shaded</b>
$A_p$	mm <sup>2</sup>	1.20 ± 0.51 <sup>a</sup>	2.94 ± 0.65 <sup>b</sup>	3.78 ± 0.27 <sup>c</sup>
$A_v$	mm <sup>2</sup>	8.21 ± 3.93 <sup>a</sup>	20.63 ± 3.64 <sup>b</sup>	26.65 ± 8.22 <sup>b</sup>
$D_a$	µm	3.67 ± 0.34	3.37 ± 0.61	3.98 ± 0.81
$D_p$	µm	9.18 ± 0.69	8.64 ± 0.55	8.89 ± 0.72
$D_v$	µm	31.22 ± 6.14 <sup>a</sup>	40.07 ± 1.98 <sup>b</sup>	42.71 ± 2.28 <sup>b</sup>
$F_c$	%	20.35 ± 2.70 <sup>a</sup>	19.01 ± 1.13 <sup>b</sup>	17.04 ± 0.96 <sup>c</sup>
$F_p$	%	15.95 ± 1.13 <sup>a</sup>	14.15 ± 0.77 <sup>b</sup>	12.53 ± 0.56 <sup>c</sup>
$F_{pf}$	%	74.45 ± 1.33	74.46 ± 2.93	74.13 ± 2.75
<b>GI</b>	-	1.84 ± 0.20 <sup>a</sup>	1.63 ± 0.05 <sup>b</sup>	1.51 ± 0.05 <sup>c</sup>
$L_p$	µm	1.99 ± 0.06	2.08 ± 0.03	1.87 ± 0.11
$L_v$	mm	70.79 ± 25.1 <sup>a</sup>	137.0 ± 18.86 <sup>b</sup>	164.6 ± 48.4 <sup>c</sup>
<b>SI</b>	%	33.13 ± 5.43 <sup>a</sup>	38.46 ± 2.19 <sup>b</sup>	43.73 ± 3.11 <sup>c</sup>
$T_m$	µm	0.26 ± 0.04	0.23 ± 0.04	0.24 ± 0.02

2 The meaning of the symbols is given in Table 1. For each trait, the method for measurement  
3 and number of replication are indicated in the methods section. Data are mean values ± standard  
4 deviation. For each line, values not followed by the same letter differ significantly at  $p < 0.05$   
5 (one-way ANOVA).

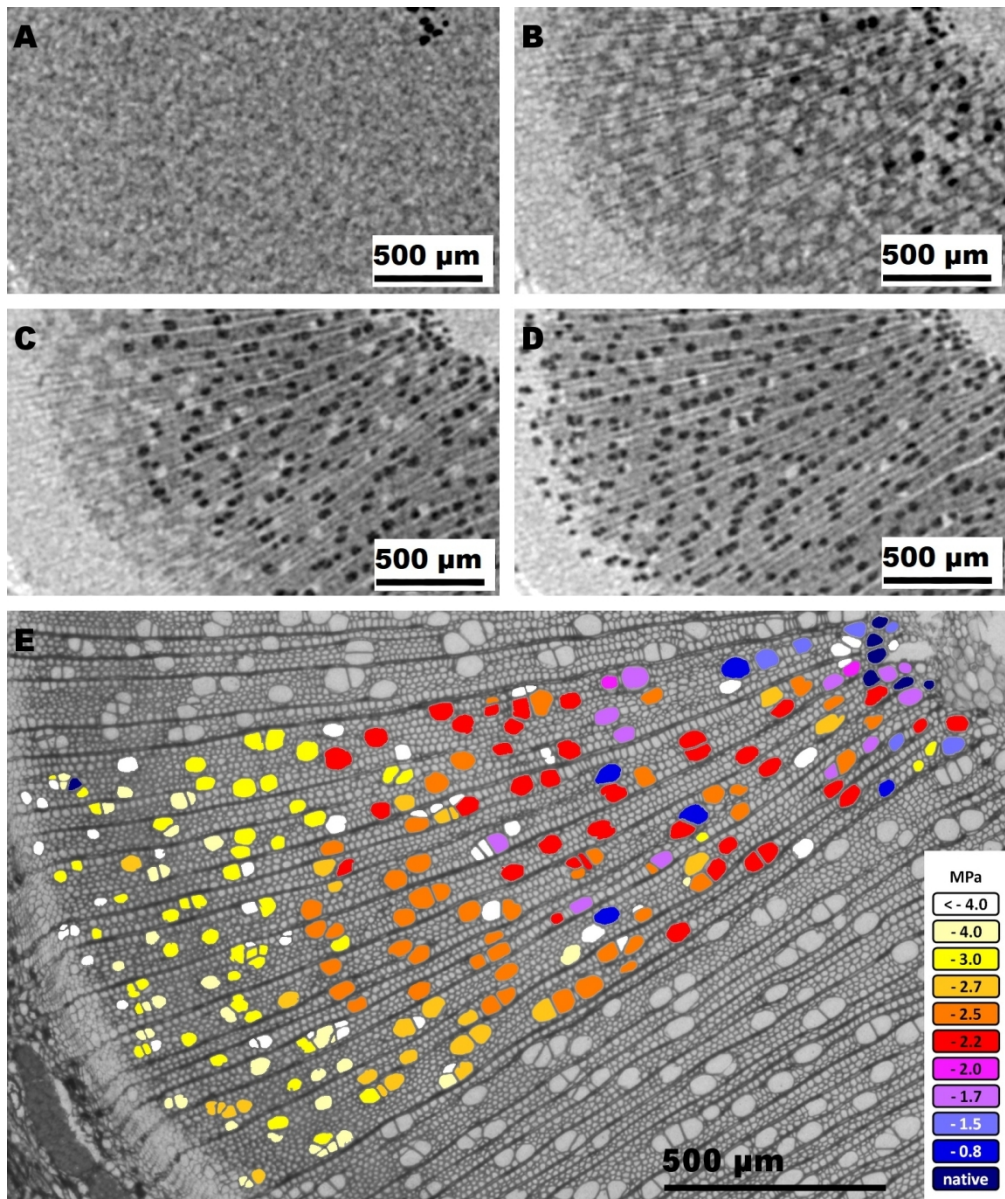


figure 1

339x404mm (120 x 120 DPI)

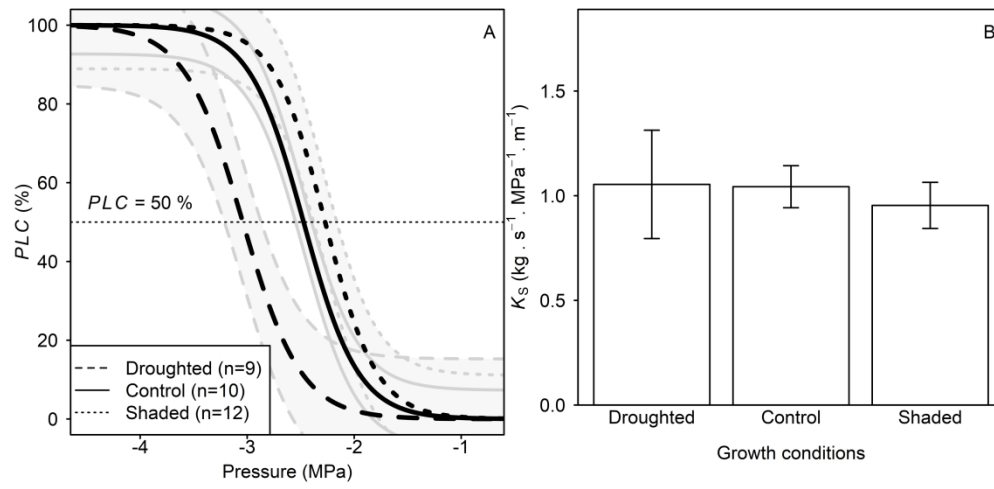


figure 2

171x82mm (600 x 600 DPI)

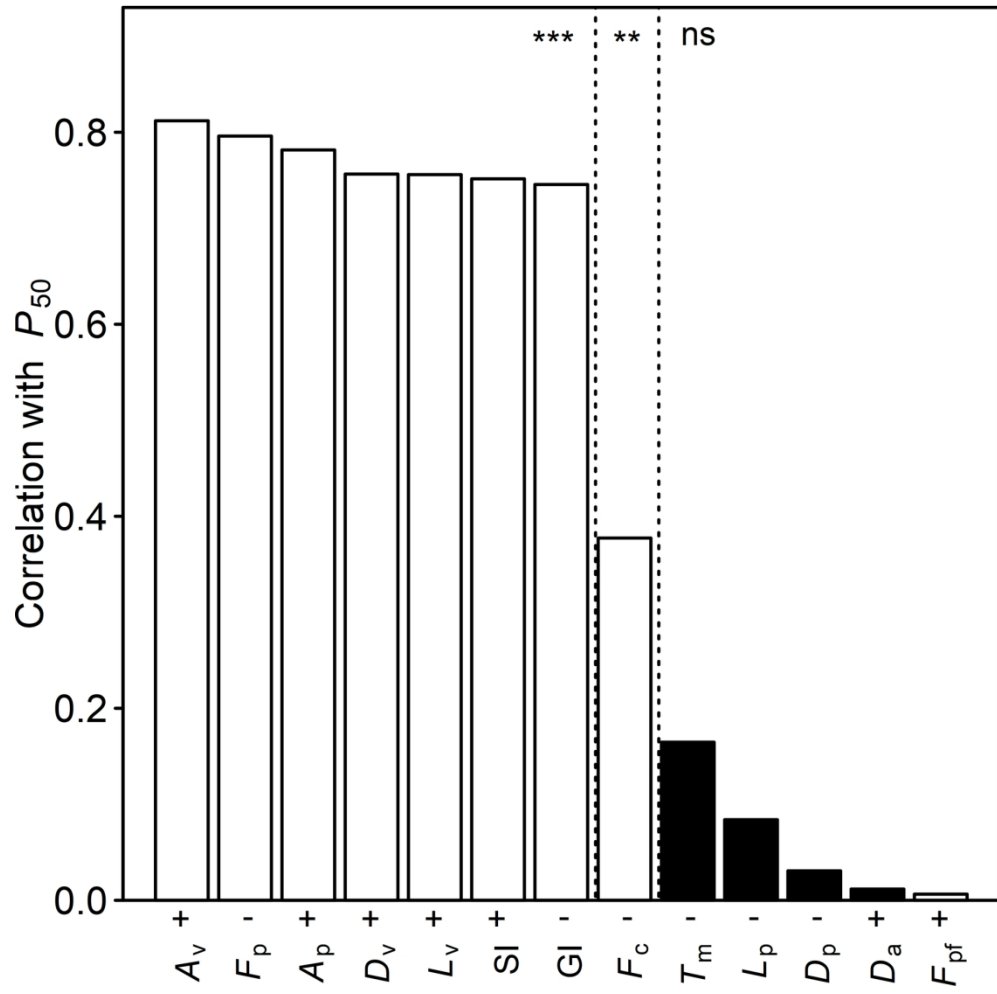


figure 3

82x82mm (600 x 600 DPI)



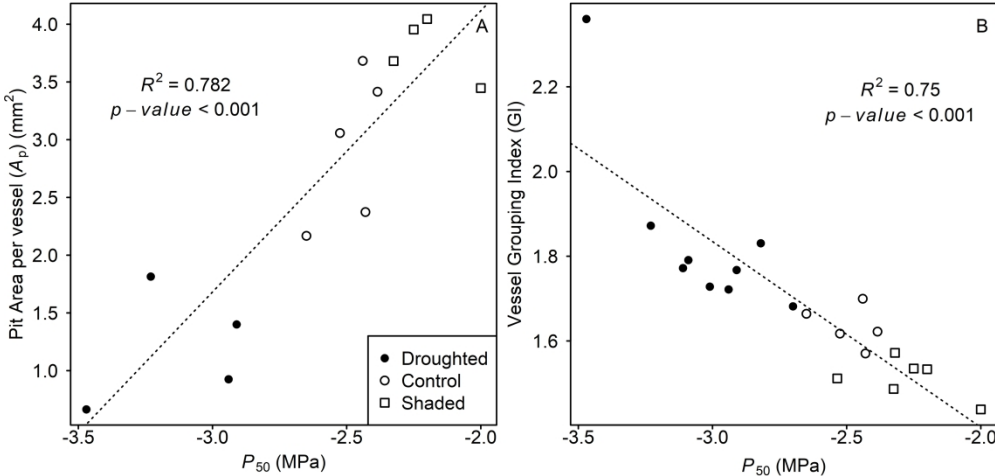


figure 4

171x82mm (600 x 600 DPI)

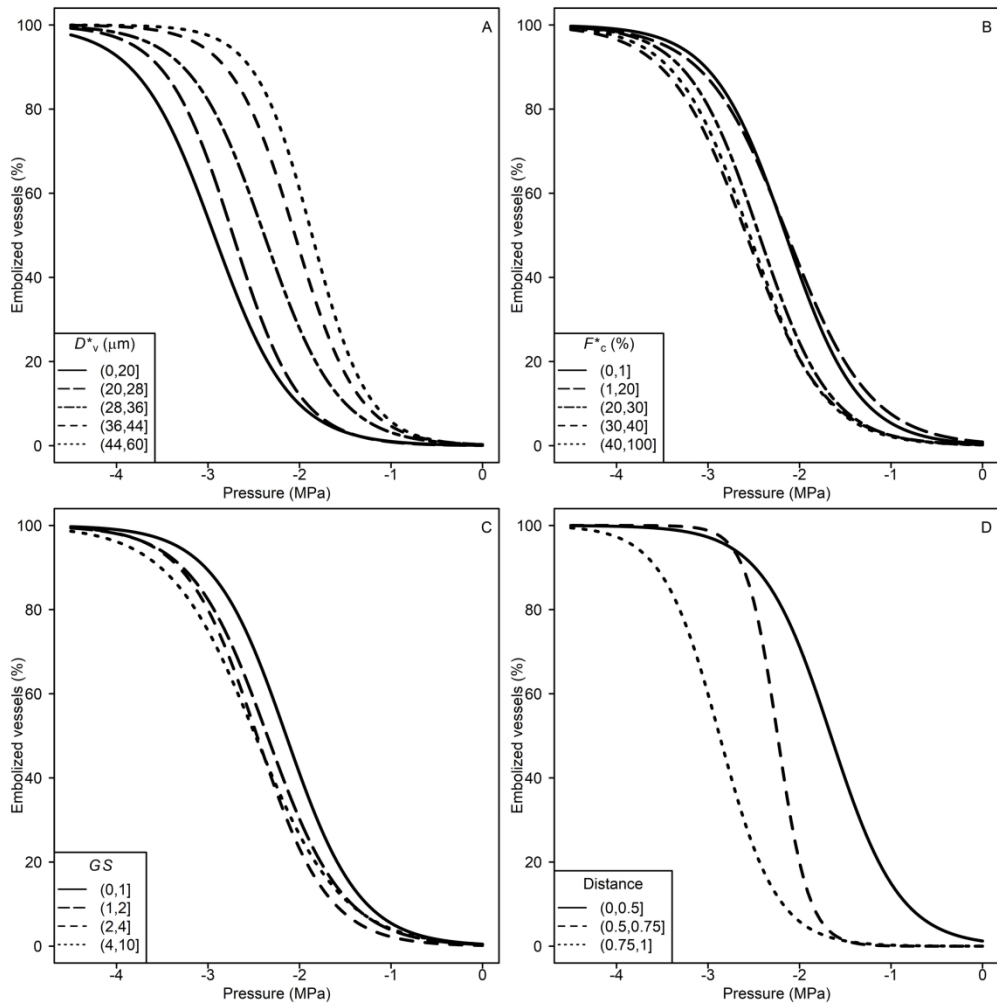


figure5

114x114mm (600 x 600 DPI)

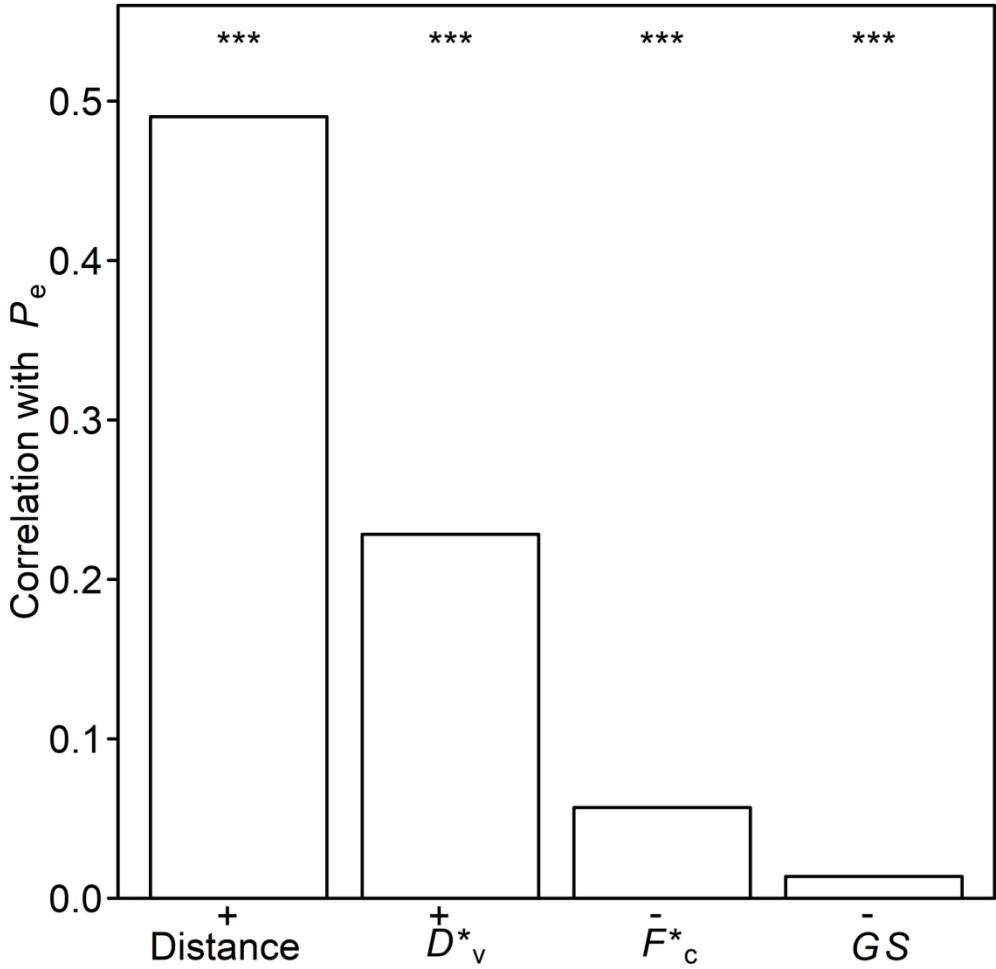


figure 6

82x82mm (600 x 600 DPI)